Analyst

PAPER

View Article Online
View Journal | View Issue

Cite this: *Analyst*, 2019, **144**, 550

Carbon nanospheres with dual-color emission and their application in ratiometric pyrophosphate sensing

Zhong-Xia Wang, Yuan-Fei Gao, Xian-He Yu, Fen-Ying Kong, Wen-Juan Wang, Wei-Xin Lv and Wei Wang*

Herein, we employ pH-dependent solubility equilibrium to develop the one-pot aqueous synthesis of dual-color emission fluorescent carbon nanosphere (DFCSs) with novel physicochemical properties. Unexpectedly, some of the DFCSs have a regular nanosphere shape, containing uniform carbon dots (~20 nm) on their surface. This may be attributed to the change in the surface composition of the carbon nanospheres under the strong alkaline conditions (pH 13), which results in dual-wavelength emission by single-wavelength excitation. Interestingly, the fluorescence intensities of the two emission peaks of the DFCSs at 315/410 nm can be simultaneously quenched upon the addition of Co^{2+} due to the strong coordination between Co^{2+} and the O-containing luminescent groups from the carbon dots and DFCSs. Also, the results demonstrate that one Co^{2+} simultaneously combines with two chromophoric groups. Furthermore, the quenched DFCSs exhibit high sensitivity for pyrophosphate (PPi) in the range of 0.075–200.0 μM through a fluorescence recovery process, which can be attributed to the stronger Co^{2+}–O=P bond. This results in the removal of Co^{2+} from the surface of DFCSs–Co^{2+} system *via* competitive adsorption interactions. Meanwhile, this sensor shows high selectivity for PPi over mercapto amino acid and phosphate in aqueous solution. These results indicate the DFCSs can act as a dual-signal PPi-selective sensor *via* a ratiometric competitive mechanism.

Received 30th August 2018,
Accepted 27th October 2018

DOI: 10.1039/c8an01676c

rsc.li/analyst

Introduction

Fluorescent analysis, which relies on special fluorescent probes for a signal readout, is one of the most acceptable techniques in the biological, bio/chemosensing, cell imaging, medical and diagnostic fields.[1,2] Compared with commonly used single-signal fluorescent probes, it is universally known that ratiometric fluorescent probes based on the relative intensity variation of two emissions can be used to determine analyte concentration accurately, improve analyte selectivity and evaluate systematic errors created by the sample environment, eliminate light collection efficiency, background interference, optical distance, sensor concentration, and light intensity.[3–7] Furthermore, ratiometric fluorescent probes can increase the dynamic range of fluorescent measurement and provide a built-in correction for environmental effects through the measurement of emission intensities at two different wavelengths.[8–11] Nowadays, studies on the ratiometric functionalization of fluorescent probes to expand their applications in chemo/biosensing are highly desirable and have attracted much attention.

Carbon-based fluorescent nanomaterials (CFNMs), as a group of newly emerging nanomaterials, have received a great deal of attention over the past three decades due to their unique characteristics, such as high photostability, low cytotoxicity, biocompatibility, outstanding fluorescence properties, ease of functionalization with biomolecules, chemical inertness and exceptional physicochemical properties.[12–14] Consequently, these glowing CFNMs can provide unprecedented opportunities for bio-imaging and optical sensing.[15–19] However, nearly all the reported CFNM probes have single-color emission by single wavelength excitation, which can decrease sensitivity and increase background interference for the analyte. Additionally, some of the major disadvantages of these nanoprobes stem from the difficulty in preparing multicolor CFNM (capable of dual-wavelength emission by single wavelength excitation) emissive products. Therefore, the development of simple methods for the preparation of water-soluble, photostable, and biocompatible, multiple-emission fluorescent nanomaterials, particularly CFNMs, is still highly desirable.

Pyrophosphate (PPi, $P_2O_7^{4-}$), which is formed by a condensation reaction between two inorganic phosphate units, is an anion that plays a central role in many biological and chemical

School of Chemistry and Chemical Engineering, Yancheng Institute of Technology, Yancheng 224051, China. E-mail: wangw@ycit.edu.cn; Fax: (+86) 515-88298186; Tel: (+86) 515-88298186

processes, including transport across membranes, cell signaling, DNA synthesis, kinase-catalysed protein phosphorylation, energy or electron-transfer processes and many enzymatic reactions.[20–22] For instance, guanosine triphosphate (GTP) and adenosine triphosphate (ATP), as nucleotides in animals and plants, are sources of chemical energy.[22,23] Also, GTP, as a general energy source, can convert to ATP in living cells, which is available for cellular functions in living systems, meanwhile, PPi can also be released in the DNA polymerization process to produce adenosine monophosphate and take part in protein synthesis and DNA replication.[23] Furthermore, it is also known that abnormal PPi levels can cause vascular calcification, leading to severe medical conditions, such as chondrocalcinosis, hypophosphatasia and calcium pyrophosphate dehydrate crystal deposition.[24,25] Therefore, the development of high sensitivity receptor-based chemosensors for the biologically important PPi anion is essential to understanding its biological activity.

Herein, we report a ratiometric chemosensor for PPi, which utilizes two distinct fluorescence signals of the same photoluminescent probe, corresponding to the simultaneous reaction of two active sites. The provided sensor shows high sensitivity and selectivity to PPi over mercapto amino acid and phosphate (Pi) in aqueous solution. Discrimination between PPi and thiol or Pi is crucial for the detection of many enzymes, thus the principle of the proposed ratiometric PPi sensing concept is shown in Scheme 1. We believe that the constructed system using a ratiometric response will provide a facile platform for the detection of PPi in serum samples and possibly in living cells.

Experimental

Materials and reagents

Adenine ($C_5H_5N_5$) was purchased from Shanghai Sangon Biological Co. Ltd (Shanghai, China). Sodium pyrophosphate ($Na_4P_2O_7{\cdot}10H_2O$, ≥99%), cobalt(II) chloride hexahydrate ($CoCl_2{\cdot}6H_2O$, ≥99%) and tris(hydroxymethyl)aminoethane (Tris) were obtained from Shanghai Sinopharm Chemical Reagents Co. Ltd (Shanghai, China). All other chemicals and solvents were of analytical grade and were used without further purification. Double distilled water was used throughout.

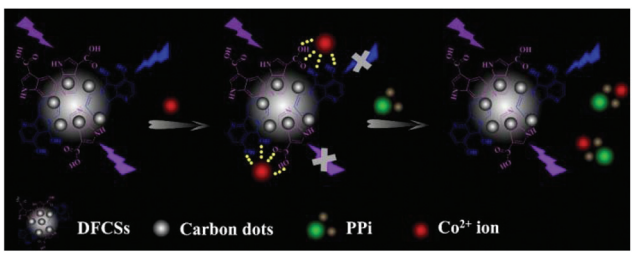

Scheme 1 Schematic diagram of the mechanism of the ratiometric detection of PPi by the proposed DFCSs–Co^{2+} metal nanocomposite.

Apparatus

UV-vis absorption spectra were recorded on a Shimadzu UV-2550 spectrophotometer (Tokyo, Japan). Photoluminescence (PL) spectra were obtained on a Jasco FP-6500 fluorescence spectrofluorometer (Jasco, Japan). Transmission electron microscopy (TEM) measurements and energy-dispersive X-ray spectroscopy (EDX) were conducted on a JEM-2100 transmission electron microscope (JEOL Ltd). X-ray photoelectron spectroscopy (XPS) analysis was performed on a Thermo ESCALAB 250 X-ray photoelectron spectrometer (USA). FT-IR spectroscopy was performed on a Nicolet 5700 (USA) IR spectrometer in the range of 400–4000 cm^{-1}. Fluorescence lifetime measurements were performed on an FL-TCSPC fluorescence spectrophotometer at the excitation wavelength of 280 nm (Horiba Jobin Yvon Inc, France).

Preparation of dual-color emission fluorescent carbon nanosphere

Dual-color emission fluorescent carbon nanospheres (DFCSs) were prepared *via* the traditional hydrothermal approach in adenine aqueous solution. Briefly, 0.15 g adenine was dissolved in 2.5 mL deionized water and 2.5 mL ethanol to form a homogeneous solution. Subsequently, the pH of the above solution was adjusted to 13 with NaOH solution (1.0 M). Then, the 5.0 mL as-prepared solution was place in a poly(tetrafluoroethylene) (Teflon)-lined autoclave and heated at 180 °C for 7.5 h, and then cooled to room temperature naturally. The water phase solution was placed in a refrigerator for about five days to remove all large DFCSs. Finally, the resulting solution was centrifuged at 10 000 rpm for 30 min to remove the large tracts, and a light-yellow DFCS aqueous solution was obtained.

Optimization of experimental conditions

To obtain a highly sensitive response for the detection of PPi, optimization of the concentration of Co^{2+} ions was carried out in our experiment. Briefly, 10 μL DFCS (8 mg mL^{-1}) stock solution was added to 50 μL Tris-HNO_3 (50 mM, pH 9.0), followed by the addition of different concentrations of Co^{2+} ions, then the final volume of the mixture was adjusted to 500 μL with double distilled water. The mixtures were equilibrated at room temperature for 30 min before PL spectroscopy measurements. The resulting solutions were studied *via* PL spectroscopy at room temperature with excitation at 280 nm, and both the excitation and emission slit widths were 5 nm.

Ratiometric fluorescent detection of PPi

The typical biomolecule detection procedure was conducted as follows. In a typical run, solutions of 50 μL Tris-HNO_3 (50 mM, pH 9.0), 10 μL DFCSs (8 mg mL^{-1}), 75 μL Co^{2+} ions (1.0 mM), and different amounts of 1.0 mM PPi solution were added in turn to a centrifuge tube (2.0 mL). Then, the mixture solution was completely mixed with a vortex mixer at room temperature for a few seconds to accelerate the chelation reaction. The final volume of the mixture was adjusted to 500 μL with double distilled water. Finally, the resulting solution was studied by PL

spectroscopy at room temperature with excitation at 280 nm, and both the excitation and emission slit widths were 5 nm.

Sensor selectivity investigation

In the selectivity experiment for PPi sensing, 10 μL of 8 mg mL^{-1} DFCSs and 75 μL of Co^{2+} ions (1.0 mM) were added to 50 μL of 50 mM Tris-HNO_3 (pH 9.0), and then a series of biomolecules and anions, including urea, cysteine (Cys), histidine (His), glutamine (Glu), SO_4^{2-}, CO_3^{2-}, HPO_4^{2-}, $H_2PO_4^-$, NO_3^-, Cl^-, SCN^-, HCO_3^-, PO_3^-, Br^- and I^- ions were added and incubated for a few seconds. The final volume of the mixture was adjusted to 500 μL with double distilled water. The mixtures were equilibrated at room temperature for 30 min before their PL spectra were recorded. The concentration of PPi and Cys was 200 μM, and the concentration of the other interference substances was 500 μM each. The resulting solutions were studied by PL spectroscopy at room temperature with excitation at 280 nm, and both the excitation and emission slit widths were 5 nm.

Results and discussion

Characterization

The DFCSs were prepared *via* a one-pot simple hydrothermal method, which is described in the Experimental section. The reaction was conducted by polymerization of adenine and ethanol in strong alkaline solution (pH 13), where they formed polymer-like organic compounds, which were then carbonized to form the DFCSs.[26] The morphology and structure of the DFCSs were confirmed by TEM analysis. Fig. 1A shows the TEM image of the DFCSs, which can be seen to have a relatively consistent particle size distribution without apparent aggregation and particle diameters of ~300 nm (inset of Fig. 1A). Meanwhile, it clearly shows that some of the DFCSs have a regular nanosphere shape containing uniform carbon dots on their surface (Fig. 1B). This may be attributed to the strong alkaline reaction conditions[27,28] and the estimated average size of the carbon dots of about 20 nm (Fig. 1B). Meanwhile, the formation of the fluorescent DFCSs was further confirmed by EDX, as shown in Fig. 1C. The EDX spectrum shows peaks corresponding to C, N, and O elements, where the content of C (35.43%), N (33.99%) and O (30.58%) elements is almost uniform in the fluorescent DFCSs (inset of Fig. 4A). However, the concentration of N element in the DFCSs is much lower than that of our previously reported carbon nanosheets prepared in neutral solution.[29] This indicates the acidity or alkalinity of the reaction surroundings has a great influence on the physicochemical properties of PL carbon-based nanomaterials.

To study the selectivity of the DFCSs for metal ions, the effect of metal ions on the PL of DFCSs was tested (Fig. 1D). High PL quenching was observed for the DFCSs upon the addition of Co^{2+} and Cu^{2+} ions, and Cd^{2+} and Mn^{2+} ions also resulted in a certain extent of quenching. Compared with the good selectivity for Ag^+ ions using the synthesized carbon nanosheets in neutral solution,[29] this poor selectivity for metal ions may be attributed to the formation of an anisotropic molecular conformation/structure in the DFCSs due to the involvement of NaOH in the synthetic process (pH 13). However, to date, there is still no convincing polymerization mechanism in strong alkaline solution for PL DFCSs.

The bonding composition and functional groups in the resultant DFCSs were characterized *via* FT-IR spectroscopy. As illustrated in Fig. 2, the peaks at about 3357, 1677, and 1515 cm^{-1} indicate the presence of the –CONH– group,[30] and the peaks at approximately 3293 and 1021 cm^{-1} correspond to the characteristic absorption bands of the –OH stretching vibration mode.[31] The characteristic absorption band of N–H stretching at 3117 cm^{-1} was also observed, and the peaks at 2973, 2797, and 845 cm^{-1} can be assigned to the C–H stretching mode and C–H out-of-plane bending mode.[32,33] Also, the

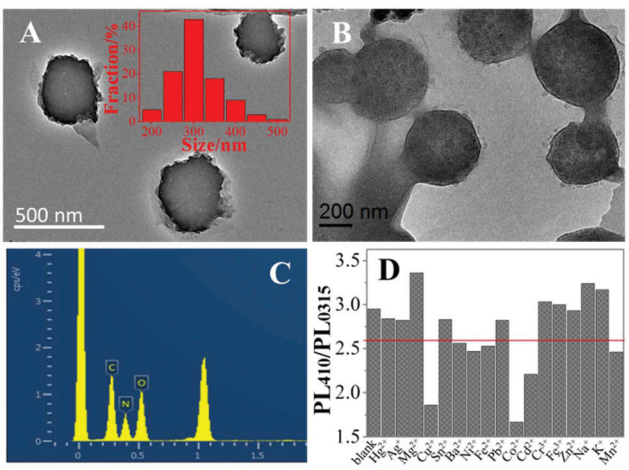

Fig. 1 TEM images (A and B) at different locations and EDX image (C) of the DFCSs. (D) Selectivity of the prepared DFCSs for the detection of metal ions, where the concentration of metal ion is 100 μM. The inset in Fig. 1A shows the diameter distribution of the DFCSs.

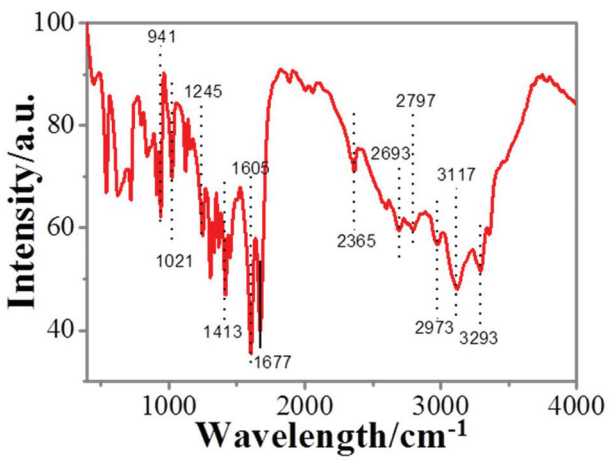

Fig. 2 FT-IR spectrum of the synthesized DFCSs under strong alkaline conditions.

characteristic absorption peaks at 1413 and 941 cm^{-1} correspond to the asymmetric stretching vibrations of the C–NH–C bands.[34,35] The aromatic C=N heterocycle stretching vibrations are observed at 1245–1605 cm^{-1}, and the C=O stretching vibration band is at 1755 cm^{-1}.[36,37] Moreover, the bands in the range of 1010–1365 cm^{-1} suggest the presence of a large number of C–O groups,[38] and the band at 831 cm^{-1} is ascribed to C–H rocking.[39]

To further explore the surface composition and elemental analysis in the hybrids, the resultant DFCSs were further characterized by XPS, as shown in Fig. 3. Compared with the synthesized carbon nanosheets in neutral solution, which contain a high concentration of N element (48.63%) and lower concentration of O element (1.72%),[29] the full range XPS analysis of the resultant DFCSs sample clearly shows the presence of C, N, and O with nearly uniform mass percentages of 35.43 wt%, 33.99 wt% and 30.58 wt% (the atomic ratio of C/N/O is 2 : 1 : 1.6), and the corresponding C 1s, N 1s, and O 1s peak centers at 284.1, 398.5, and 531.9 eV, respectively (Fig. 3A). Based on the Shirley algorithm, the high-resolution N 1s spectrum (Fig. 3B) exhibits three main peaks at 398.7, 398.5 and 399.4 eV, which are attributed to the N in a graphite-like structure, pyridinic-type N and pyrrolic-type N groups,[19,40,41] respectively. This indicates that the DFCSs are rich in N in C=N/N=N and C–N groups on their surfaces, which were observed in the FT-IR spectrum (Fig. 2). Also, the three peaks at 530.7, 531.5, and 535.2 eV in the O 1s spectrum (Fig. 3C) are attributed to C=O, C–OH, and C–O–C groups,[29,33,42] respectively. The high-resolution C 1s spectrum shows four main peaks (Fig. 3D). The peak at a binding energy of 284.3 eV confirms the graphitic structure (sp^2 C=C) of the DFCSs,[24] and the peaks at about 285.2 and 286.2 eV suggest the presence of C–N and C–O groups on the surface of the DFCSs, respectively. Additionally, the peak at around 288.2 eV can be assigned to C=O and C=N groups,[29,43] indicating that the prepared DFCSs are rich in hydroxyl, carbonyl, carboxylic acid and N-containing groups on their surfaces, which are consistent with the corresponding FT-IR result. Therefore, the presence of polycyclic heterocyclic aromatic containing C=N/C–N species and hydroxyl, carbonyl and carboxylic moieties on the surface of DFCSs was confirmed by the XPS and FT-IR results. All these observations indicate that these nanospheres are quite different from previously reported carbon materials.

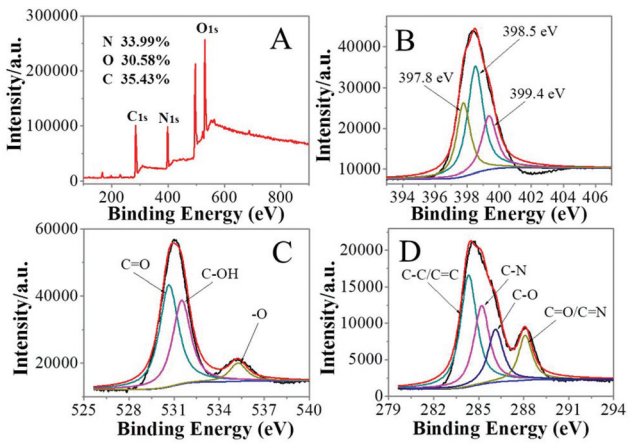

Fig. 3 XPS (A), N 1s (B), O 1s (C), and C 1s (D) spectra of the obtained DFCSs.

Investigation of the properties of the DFCSs

To investigate the optical properties of the obtained DFCSs, their UV-vis absorption and excitation-independent PL behavior were investigated. Fig. 4A shows the absorption and emission spectra of the obtained DFCSs (curves a and b, respectively). Fig. 4A shows that the DFCSs suspension has a typical UV-vis absorption peak at 261 nm with a weak shoulder at 280 nm (curve a). The absorption peak at approximately 261 nm is assigned to the σ–π and π–π* transitions originating from the C=C and C=N groups at the zigzag edges of the carbon nanospheres and confirms the existence of aromatic N-containing heterocycles.[44,45] This leads to almost no observed PL signal and suggests that the PL DFCSs are not produced by electronic conjugate structures.[46] Furthermore, the other transition centered at about 280 nm is due to the n–π* electron transition of C=O[47] (curve c, Fig. 4A), that is, the trapping of excited-state energy by the surface states, which results in strong emission.[47,48] Meanwhile, it is noted that the DFCS solution shows two strong PL emission peaks centered at 315 nm and 420 nm upon single excitation at 280 nm (Fig. 4A, curve b). Unlike most carbon nanomaterials, the peak position of the PL emission of the DFCSs at 315 nm and 420 nm does not change upon varying the excitation wavelength from 270 nm to 285 nm (Fig. 4B), which can be attributed to the two "self-passivated" activated chromophoric groups on the surface of the DFCSs, leading to the formation of surface states between the π* band and π electron energy level.[49] That is, the emission wavelength of the DFCSs is independent of the excitation wavelength (when the excitation wavelength was changed from 270 nm to 285 nm, the emission wavelength showed nearly no shift; Fig. 4B). However, considering the construction of a proportional sensor, the optimum excitation wavelength and emission wavelength of the DFCS aqueous solution are 280 and 315/410 nm, respectively, which indicate

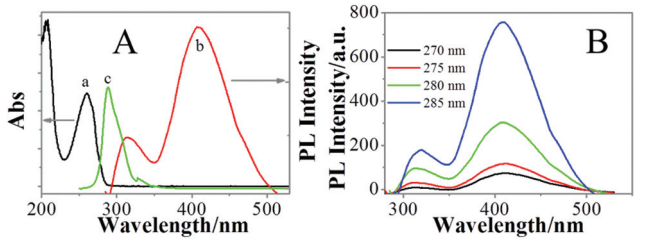

Fig. 4 (A) UV-vis absorption (curve a), emission (curve b, λ_{em} = 315 and 410 nm) and excitation (curve c, λ_{ex} = 280 nm) spectra of the DFCSs. (B) PL spectra of the DFCSs at different excitation wavelengths ranging from 270 to 285 nm, where both the excitation and emission slit widths were 5 nm.

the prepared DFCSs possess a uniform distribution of surface states.[36,50]

Optimization of experimental conditions

From the experimental results, it is noted that PL quenching process by Co^{2+} ions is the best quenching effect, and the PL quenching process may be pH-dependent due to the nature of the carboxyl and hydroxyl groups (–COOH and –OH) on the surface of the DFCSs. Therefore, to maximize their signal and detection sensitivity for PPi, we investigated the effect of pH on the detection of the Co^{2+} ions and PPi, as shown in Fig. 5A. Fig. 5A shows the PL responses of the DFCSs to 100 μM Co^{2+} ions or 150 μM Co^{2+} ion and 50 μM PPi at various pH values.

Here, fluctuating pH values in the range of 7.0–9.5 (Tris-HNO_3, 5 mM) were investigated (Fig. 5A, curve a). The ratio signal ($PL_{410\ nm}/PL_{0315\ nm}$) decreased with an increment in pH value from pH 7.0–9.0 and then increased quickly when the pH was over 9.0. Also, it can clearly be seen that recovery efficiency of the PL of the DFCS increased gradually as the pH increased from 7.0 to 9.0, and then it decreased gradually as the pH increased (Fig. 5A, curve b). This can be explained by the fact that lowly or highly alkaline surroundings would damage the configuration of the carboxyl and carbonyl moieties by protonation–deprotonation reaction, which greatly affects the interaction between the DFCSs and Co^{2+} ions or Co^{2+} ions and PPi. Therefore, pH 9.0 was selected as the optimum pH value for the detection of PPi.

Mechanism of PPi detection by DFCSs

Co^{2+} ions, as an unusual quencher, can quench the fluorescence of organic fluorescent microcrystals[51] and fluorescent carbon-based materials[52,53] through electronic transfer or other processes. Also, it is well-known that Co^{2+} ions are an acid of borderline hardness (according to the hard and soft acids and bases principle), which have strong affinity for oxygen and nitrogen donor atoms. As a result, transition-state chelates are formed between Co^{2+} ions and the O/N atoms in the DFCSs. Meanwhile, Co^{2+} ions are known to be a Lewis acid and, therefore, have strong affinity to accept electrons (according to the Lewis acid–base theory). Thus, Co^{2+} ions were slowly added to the PL DFCSs under the excitation state and the electron, which was transferred in the DFCSs by the Co^{2+} ion is back-donated in the vacant orbital of the Co^{2+} ion, leading to a strong electronic interaction,[19] thereby decreasing its luminescence intensity. Furthermore, the Co^{2+} ions can strongly react with the carboxyl and carbonyl moieties of compounds *via* effective coordination/chelation interactions,[52,54] which leads to significant PL recovery of quenched PL nanomaterials by Co^{2+} ions. Based on this, the feasibility of the newly developed PL turn on–off–on DFCSs was evaluated by the addition of Co^{2+} ions and PPi. As shown in Fig. 5B, the double emission peaks at 410/315 nm of the DFCSs were significantly quenched in the presence of Co^{2+} ions due to the strong coordination between the Co^{2+} ions and O-containing groups on the surface of the DFCSs (Fig. 5B, curve b). However, owing to the stronger affinity between PPi and Co^{2+} ions than that of the O-containing groups on the surface of the DFCSs, the continual addition of PPi restored the PL due to the competition between PPi and the O-containing groups to coordinate with Co^{2+} ions, leading to the re-dispersion of DFCSs (Fig. 5B, curve c). Specifically, the DFCSs have a strong PL emission peaks at 410/315 nm when excited at 280 nm (Fig. 5B, curve a); however, the PL emission peaks at 410/315 nm were strongly quenched upon the addition of 150 μM Co^{2+} ions. The quenching efficiency reached nearly 68% (Fig. 5B, curve b), whereas the addition of PPi to the mixture solution regenerated the PL intensity up to 96% of its initial value (Fig. 5B, curve c). The recovery of PL intensity is based on the stronger coordination/chelation interactions between the Co^{2+} ions and the abundant P=O groups of PPi.[55] Thus, these results demonstrate that DFCSs–Co^{2+} assemblies can effectively serve as a promising ratiometric sensing platform for the detection of PPi, where the DFCSs function as the fluorometric probe and Co^{2+} ions act bifunctionally as the PL quencher and PPi recognizer. Furthermore, it was noted that the pH of the reaction solution affects the physical and chemical properties of carbon-based nanomaterials, which plays an important role in during the synthetic process.

The Co^{2+} ion concentration affects not only the PL intensity but also the sensitivity of the PPi assay. Therefore, to obtain high sensitivity and quenching effect on the PL intensity of DFCSs in the presence of Co^{2+} ions, various concentrations of dispersed Co^{2+} ions were added to identical aliquots of DFCSs (Fig. 6A and B). Fig. 6A shows the PL intensity of the DFCSs in the presence of various concentrations of Co^{2+} ions ranging from 20 to 200 μM. It is clearly shown that the PL emission peaks at 410/315 nm for the DFCSs were gradually quenched as the concentration of Co^{2+} ions increased, and the maximum quenching efficiency reached nearly 68% when the Co^{2+} ion concentration was 150 μM (Fig. 6B, black dots). This large decrease in PL intensity may be attributed to the specifically combined conformation formed by two fluorescent chromophores formed through the hydroxyl, carbonyl and carboxylic acid groups on the surfaces of the DFCSs, which bind to the Co^{2+} ions. Furthermore, it is worth noting that the basically unchanged PL ratiometric value at $PL_{410\ nm}/PL_{315\ nm}$ for the DFCSs in the presence of various concentrations of Co^{2+} ion

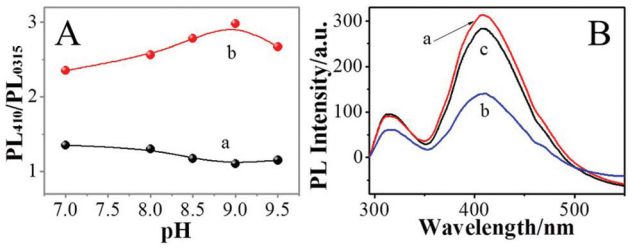

Fig. 5 (A) Plot of the PL signals $PL_{410\ nm}/PL_{0315\ nm}$ of the DFCSs in different pH value Tris-HNO_3 buffer in the presence of Co^{2+} ions (curve a) or Co^{2+} ions and PPi (curve b), where the concentration of Co^{2+} ions and PPi is 100 μM, 150 μM and 50 μM, respectively. (B) PL emission spectrum (λ_{ex} = 280 nm) of free DFCSs (curve a) and DFCSs in the presence of Co^{2+} ions (curve b), and both Co^{2+} ions and PPi (curve c).

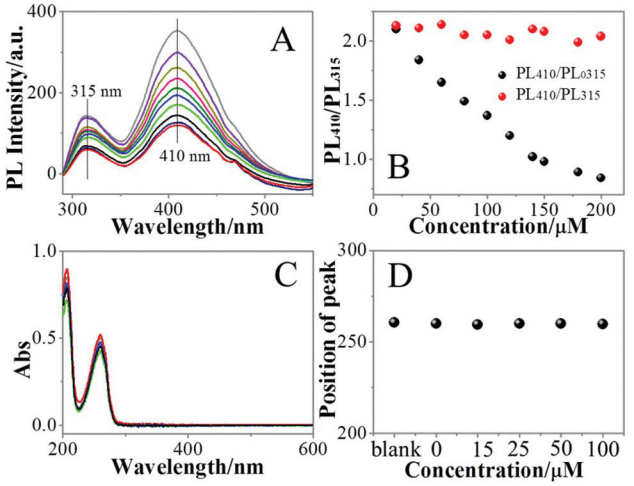

Fig. 6 (A) PL emission spectra of the DFCSs in the presence of different concentrations of Co^{2+} ions (top to bottom, excitation at 280 nm). (B) Plot of the PL signals $PL_{410\ nm}/PL_{315\ nm}$ *versus* Co^{2+} ion concentration. The black dots stand for the PL signals $PL_{410\ nm}/PL_{315\ nm}$ *versus* Co^{2+} ion concentration and the red dots for the PL signals $PL_{410\ nm}/PL_{315\ nm}$ *versus* Co^{2+} ion concentration, concentration: Tris-HNO_3 buffer, 5 mM; λ_{ex}, 280.0 nm. (C) UV-vis spectra of DFCSs (160 μg mL^{-1}), DFCSs (160 μg mL^{-1}) + Co^{2+} ion (150 μM), and DFCSs (160 μg mL^{-1}) + Co^{2+} ion (150 μM) in the presence of different concentrations of PPi (15 μM, 25 μM, 50 μM and 100 μM, respectively). (D) Plot of the location of the characteristic absorption peak at about 260 nm *versus* blank, Co^{2+} ion or Co^{2+} ion and PPi.

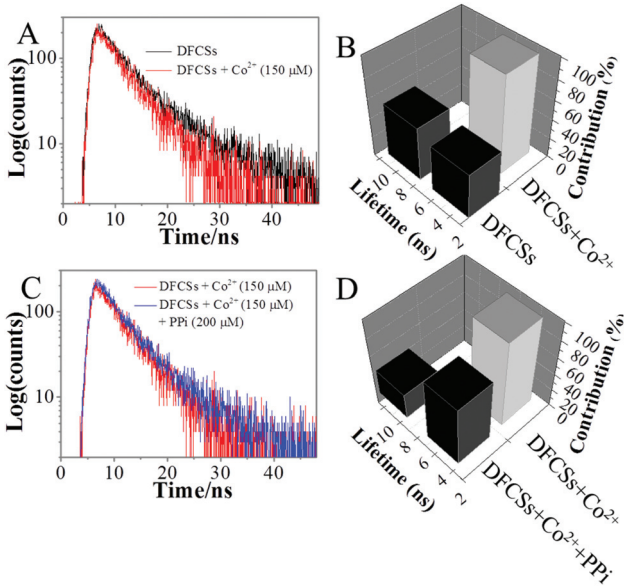

Fig. 7 (A) and (C) Decay of the PL of the DFCSs in the absence and presence of Co^{2+} ions, and Co^{2+} ions and PPi, respectively. (B) and (D) PL lifetimes of the DFCSs in the absence and presence of Co^{2+} ions, and Co^{2+} ions and PPi, respectively. The concentration of Co^{2+} ions and PPi was 150 μM and 200 μM, respectively.

illustrates that each Co^{2+} ion simultaneously combines two chromophoric groups of the DFCSs (Fig. 6B, red dots). Based on the results, 150 μM was selected as the optimal Co^{2+} ion concentration for the subsequent experiments (Fig. 6B).

To reveal the mechanism of how the PL changes, the time-resolved PL spectra of the DFCSs, DFCSs–Co^{2+} complexes and DFCSs–Co^{2+} complexes in the presence of PPi were measured. Due to the differences in the distribution of the complex luminescent pathways resulting from multiple DFCSs species and/or sites,[56] the PL intensity of the DFCSs followed dual-exponential decay kinetics and two lifetimes were acquired (Fig. 7). As shown in Fig. 7B and D, it was found that the PL lifetime of the DFCSs greatly change in a very obvious manner with the addition of Co^{2+} ions or Co^{2+} ions and PPi. These large changes in the PL lifetime of the DFCSs can be attributed to the increase in the radiative decay rates, indicating that the formation of an extra shell partly through combination with Co^{2+} ions destroys the surface defects. Meanwhile, the nonlinear Stern–Volmer plots (Fig. 6B, black dots) indicate that the decrease in lifetime of the DFCSs by Co^{2+} ions obeys a simple dynamic quenching mechanism, which was further confirmed by the UV-vis absorbance spectra (Fig. 6C and D). That is, the Co^{2+} ion, unlike Eu^{3+} ion,[56] coordinating to the oxygen-donor atoms of the carboxyl and carbonyl groups on the surface of the DFCSs, should not act as a bridge to link neighboring carboxylate groups, and the subsequent quenching of PL of DFCSs in the presence of Co^{2+} ion might be attributed to the electron or energy transfer mechanism.[19,57]

Ratiometric detection of PPi using DFCSs as probes

Considering the effective coordination/chelation reaction between Co^{2+} ions and the active O-containing groups (*e.g.*, C═O) in carbon nanospheres,[54] the DFCSs–Co^{2+} assembly system was utilized to detect the P═O of PPi under the optimized conditions (Tris-HNO_3 buffer of pH 9.0 and Co^{2+} ions: 150 μM). Fig. 8A shows the PL recoveries of the DFCSs–Co^{2+} system with an increasing concentration of PPi, and it can be clearly seen that the PL was gradually restored as more and more PPi was added. Upon adding PPi (150 μM) to the DFCSs–Co^{2+} assembly system, the PL of the DFCSs was nearly completely restored, revealing that the sensing system is very sensitive to PPi concentration. The reason for the PPi recovery may be as follows: a stronger Co^{2+}–O═P bond can be formed between the Co^{2+} ion and PPi, resulting in the removal of the Co^{2+} ion from the surface of the DFCSs-Co^{2+} system *via* competitive adsorption interactions (Scheme 1),[55,58] which enhanced the

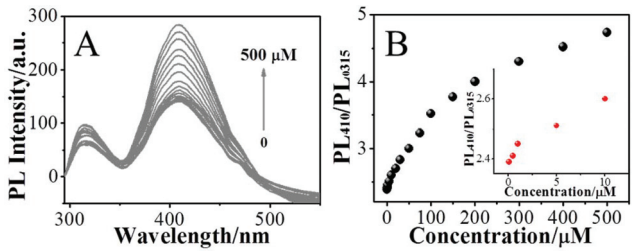

Fig. 8 (A) PL recovery of the DFCSs–Co^{2+} assembly in the presence of different concentrations of PPi (0 to 500 μM, bottom to top, excitation at 280 nm). (B) Plot of the enhanced PL signals $PL_{410\ nm}/PL_{0315\ nm}$ *versus* PPi concentration.

PL of the DFCSs–Co^{2+} nanocomposite. In the range of 0.075–200.0 μM, the increased PL of the DFCSs showed a good linear relationship to the concentration of PPi with a correlation coefficient of 0.9902 (n = 5) (Fig. 8B), and the detection limit for PPi was calculated to be 25.76 nM ($3\sigma/k$), which is much lower than that of previously reported sensors.[55,58–61]

Selectivity of the DFCS probe

Besides sensitivity, selectivity is another important parameter to evaluate the performance of the sensing system. Thus, under the optimal conditions (Tris-HNO_3 buffer of pH 9.0 and Co^{2+} ions: 150 μM), we tested the PL intensity changes of the DFCSs–Co^{2+} assembly in the presence of competitive biomolecules and anions under the same conditions, including urea, cysteine (Cys), histidine (His), glutamine (Glu), SO_4^{2-}, CO_3^{2-}, HPO_4^{2-}, $H_2PO_4^-$, NO_3^-, Cl^-, SCN^-, HCO_3^-, PO_3^-, Br^- and I^- ions, as shown in Fig. 9. It was observed that the relative PL ratiometric intensity of $PL_{410\ nm}/PL_{0315\ nm}$ was enhanced the most by PPi, and in contrast, the PL of other detected biomolecules and anions showed no significant increase even when their concentrations were 2.5-fold higher than that of PPi (the PL intensities of DFCSs–Co^{2+} in the absence and presence of other biomolecules are denoted by $PL_{0315\ nm}$ and $PL_{410\ nm}$, respectively). This illustrates the high selectivity of the developed on–off–on sensor, which has potential use for the determination of PPi in real samples. Therefore, the PPi contents in real bovine serum samples were detected to further illustrate its feasibility. The proposed method was applied for the analysis of PPi in three bovine serum samples obtained from Shanghai Sinopharm Chemical Reagents Co. Ltd (Shanghai, China) by the standard addition method, and the results are shown in Table 1. From Table 1, the standard deviations and recovery (95.56–104.89%) with less than 5.0% RSD under the optimal conditions demonstrate the effectiveness of the proposed method for the detection of PPi. The results also prove the high selectivity and sensitivity of the DFCSs–Co^{2+} system for the detection of PPi, indicating that this sensor has potential applicability for real sample analysis.

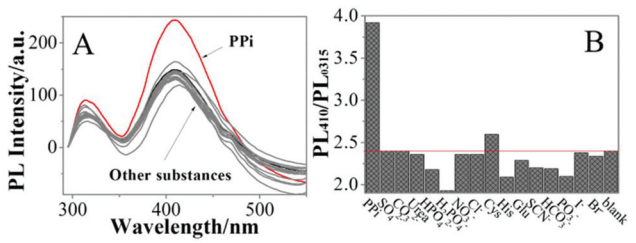

Fig. 9 (A) PL emission spectra of the DFCSs–Co^{2+} nanocomposite in the presence of various interfering substances in 5 mM Tris-HNO_3 buffer (pH 9.0). (B) Selectivity of the PL assay for PPi over other ions. The concentration of PPi was 200 μM. The concentration of the other interfering substances was 500 μM except for Cys which was 200 μM.

Table 1 Analytical results for the determination of PPi in bovine serum samples (1%) using the proposed DFCSs–Co^{2+} metal nanocomposite

Sample	Anions	Added[a] (μM)	Measured[a] (μM)	Recovery (%)	RSD (n = 3, %)
Sample1	PPi	50	47.89	95.79	3.36
Sample2	PPi	100	95.56	95.56	4.89
Sample3	PPi	150	157.34	104.89	3.73

[a] The data was obtained from three parallel samples.

Conclusion

In summary, DFCSs with pH-controlled physicochemical properties were obtained through a simple, one-pot, hydrothermal approach from adenine under a strongly alkaline environment. The results indicate that acid and alkaline environments in the reacting precursor solution play an important role in determining the molecular structure and physicochemical properties of the DFCSs. Next, we presented the development of a multiplex, specific, indirect, continuous and ratiometric PPi assay based on the stronger Co^{2+}–O═P bond formed between Co^{2+} ions and PPi, resulting in the removal of Co^{2+} ions from the surface of the non-PL DFCSs–Co^{2+} system *via* competitive adsorption interactions, and therefore successfully attained the ultrasensitive detection of PPi with a detection limit of 25.76 nM. Under the optimal conditions, the on–off–on sensor displays a wide linear range and good selectivity over other biomolecules and anions. Furthermore, the concentration of PPi in bovine serum samples was successfully detected with the newly developed off–on PL sensor, and the standard deviations and recoveries (95.56–104.89%) demonstrated the good repeatability and high accuracy of the sensor, which fulfills the requirements for real-time applications. The simultaneous possession of high sensitivity and selectivity, rapidity, and convenience enables this off–on sensor to be potentially applicable for the ultrasensitive and rapid on-site detection of trace PPi.

Conflicts of interest

There are no conflicts to declare.

Acknowledgements

This we greatly appreciate the support of the National Natural Science Foundation of China (21705140, 21575123, 21675139, 21603184) and the Natural Science Foundation of Jiangsu Province (BK20170474) and the sponsorship from the Qing Lan Project. We appreciate the support of the opening project of Jiangsu Key Laboratory of Biochemistry and Biotechnology of Marine Wetland (K2016-17, K2016-20).

Notes and references

1 J. Sun, H. Mei and F. Gao, *Biosens. Bioelectron.*, 2017, **91**, 70–75.

2 W. C. Chan and S. Nie, *Science*, 1998, **281**, 2016–2018.
3 Q. Han, Z. Mou, H. Wang, X. Tang, Z. Dong, L. Wang, X. Dong and W. Liu, *Anal. Chem.*, 2016, **88**, 7206–7212.
4 Z. Xu, Y. Xiao, X. Qian, J. Cui and D. Cui, *Org. Lett.*, 2005, **7**, 889–892.
5 J. Sun, S. Wang and F. Gao, *Langmuir*, 2016, **32**, 12725–12731.
6 W. Lin, L. Long, B. Chen and W. Tan, *Chem. – Eur. J.*, 2009, **15**, 2305–2309.
7 Q. Zhao, F. Li and C. Huang, *Chem. Soc. Rev.*, 2010, **39**, 3007–3030.
8 Y. Kubo, M. Yamamoto, M. Ikeda, M. Takeuchi, S. Shinkai, S. Yamaguchi and K. Tamao, *Angew. Chem., Int. Ed.*, 2003, **42**, 2036–2040.
9 J. Raker and T. E. Glass, *J. Org. Chem.*, 2002, **67**, 6113–6116.
10 H. Fu, B. H. Loo, D. Xiao, R. Xie, X. Ji, J. Yao, B. Zhang and L. Zhang, *Angew. Chem., Int. Ed.*, 2002, **41**, 962–965.
11 H. Takakusa, K. Kikuchi, Y. Urano, S. Sakamoto, K. Yamaguchi and T. Nagano, *J. Am. Chem. Soc.*, 2002, **124**, 1653–1657.
12 M. Kawamoto, P. He and Y. Ito, *Adv. Mater.*, 2017, **29**, 1602423.
13 V. Georgakilas, J. A. Perman, J. Tucek and R. Zboril, *Chem. Rev.*, 2015, **115**, 4744–4822.
14 S. Zhu, Q. Meng, L. Wang, J. Zhang, Y. Song, H. Jin, K. Zhang, H. Sun, H. Wang and B. Yang, *Angew. Chem., Int. Ed.*, 2013, **52**, 3953–3957.
15 L. Chen, G. Yang, P. Wu and C. Cai, *Biosens. Bioelectron.*, 2017, **96**, 294–299.
16 L. L. Feng, Y. X. Wu, D. L. Zhang, X. X. Hu, J. Zhang, P. Wang, Z. L. Song, X. B. Zhang and W. Tan, *Anal. Chem.*, 2017, **89**, 4077–4084.
17 K. Jiang, S. Sun, L. Zhang, Y. Lu, A. Wu, C. Cai and H. Lin, *Angew. Chem., Int. Ed.*, 2015, **54**, 5360–5363.
18 Z. X. Wang, F. Y. Kong, W. J. Wang, R. Zhang, W. X. Lv, X. H. Yu and W. Wang, *Sens. Actuators, B*, 2017, **242**, 412–417.
19 Z. X. Wang and S. N. Ding, *Anal. Chem.*, 2014, **86**, 7436–7445.
20 X. Zhao and K. S. Schanze, *Chem. Commun.*, 2010, **46**, 6075–6077.
21 S. K. Kim, D. H. Lee, J. I. Hong and J. Yoon, *Acc. Chem. Res.*, 2009, **42**, 23–31.
22 Z. Zeng, A. A. J. Torriero, A. M. Bond and L. Spiccia, *Chem. – Eur. J.*, 2010, **16**, 9154–9163.
23 J. R. Knowles, *Annu. Rev. Biochem.*, 1980, **49**, 877–919.
24 Z. X. Wang, X. H. Yu, F. Li, F. Y. Kong, W. X. Lv and W. Wang, *J. Mater. Chem. B*, 2018, **6**, 1771–1781.
25 L. Hessle, K. A. Johnson, H. C. Anderson, S. Narisawa, A. Sali, J. W. Goding, R. Terkeltaub and J. L. Millán, *Proc. Natl. Acad. Sci. U. S. A.*, 2002, **99**, 9445–9449.
26 X. Xiang, Z. Zhang, L. Han, F. Huang, M. Zheng, H. Tang and Q. Deng, *Sens. Actuators, B*, 2017, **241**, 482–488.
27 Z. X. Wang, X. H. Yu, F. Li, F. Y. Kong, W. X. Lv, D. H. Fan and W. Wang, *Microchim. Acta*, 2017, **184**, 4775–4783.
28 S. Lu, R. Cong, S. Zhu, X. Zhao, J. Liu, J. S. Tse, S. Meng and B. Yang, *ACS Appl. Mater. Interfaces*, 2016, **8**, 4062–4068.
29 Z. X. Wang, F. Y. Kong and W. Wang, *Chem. – Eur. J.*, 2017, **23**, 665–675.
30 J. Deng, Q. Lu, Y. Hou, M. Liu, H. Li, Y. Zhang and S. Yao, *Anal. Chem.*, 2015, **87**, 2195–2203.
31 M. J. Bojdys, J. O. Muller, M. Antonietti and A. Thomas, *Chem. – Eur. J.*, 2008, **14**, 8177–8182.
32 Z. L. Wu, P. Zhang, M. X. Gao, C. F. Liu, W. Wang, F. Leng and C. Z. Huang, *J. Mater. Chem. B*, 2013, **1**, 2868–2873.
33 W. Lu, X. Qin, S. Liu, G. Chang, Y. Zhang, Y. Luo, A. M. Asiri, A. O. Al-Youbi and X. Sun, *Anal. Chem.*, 2012, **84**, 5351–5357.
34 L. Wang, S. J. Zhu, H. Y. Wang, S. N. Qu, Y. L. Zhang, J. H. Zhang, Q. D. Chen, H. L. Xu, W. Han, B. Yang and H. B. Sun, *ACS Nano*, 2014, **8**, 2541–2547.
35 L. Zhang, D. Peng, R. P. Liang and J. D. Qiu, *Chem. – Eur. J.*, 2015, **21**, 9343–9348.
36 Y. Dong, H. Pang, H. B. Yang, C. Guo, J. Shao, Y. Chi, C. M. Li and T. Yu, *Angew. Chem., Int. Ed.*, 2013, **52**, 7800–7804.
37 M. Rong, Y. Liang, D. Zhao, B. Chen, C. Pan, X. Deng, Y. Chen and J. He, *Sens. Actuators, B*, 2018, **265**, 498–505.
38 X. Jia, J. Li and E. K. Wang, *Nanoscale*, 2012, **4**, 5572–5575.
39 Y. Wang, Q. Zhuang and Y. Ni, *Chem. – Eur. J.*, 2015, **21**, 13004–13011.
40 Y. Q. Zhang, D. K. Ma, Y. Zhuang, X. Zhang, W. Chen, L. L. Hong, Q. X. Yan, K. Yu and S. M. Huang, *J. Mater. Chem.*, 2012, **22**, 16714–16718.
41 K. P. Gong, F. Du, Z. H. Xia, M. Durstock and L. M. Dai, *Science*, 2009, **323**, 760–764.
42 H. Zhang, Y. Li, X. Liu, P. Liu, Y. Wang, T. An, H. Yang, D. Jing and H. Zhao, *Environ. Technol. Lett.*, 2014, **1**, 87–91.
43 Y. Li, Y. Zhao, H. Cheng, Y. Hu, G. Shi, L. Dai and L. Qu, *J. Am. Chem. Soc.*, 2012, **134**, 15–18.
44 Y. Li, Y. Hu, Y. Zhao, G. Q. Shi, L. E. Deng, Y. B. Hou and L. Qu, *Adv. Mater.*, 2011, **23**, 776–780.
45 A. Ananthanarayanan, X. Wang, P. Routh, B. Sana, S. Lim, D. H. Kim, K. H. Lim, J. Li and P. Chen, *Adv. Funct. Mater.*, 2014, **24**, 3021–3026.
46 G. Eda, Y. Lin, C. Mattevi, H. Yamaguchi, H. Chen, I. Chen, C. W. Chen and M. Chhowalla, *Adv. Mater.*, 2010, **22**, 505–508.
47 X. Wang, L. Cao, S. T. Yang, F. Lu, M. J. Meziani, L. Tian, K. W. Sun, M. A. Bloodgood and Y. P. Sun, *Angew. Chem., Int. Ed.*, 2010, **49**, 5310–5314.
48 X. Liu, H. Jiang, J. Ye, C. Zhao, S. Gao, C. Wu, C. Li, J. Li and X. Wang, *Adv. Funct. Mater.*, 2016, **26**, 8694.
49 L. Tang, R. Ji, X. Cao, J. Lin, H. Jiang, X. Li, K. S. Teng, C. M. Luk, S. Zeng, J. Hao and S. P. Lau, *ACS Nano*, 2012, **6**, 5102–5110.
50 Y. P. Sun, B. Zhou, Y. Lin, W. Wang, K. A. S. Fernando, P. Pathak, M. J. Meziani, B. A. Harruff, X. Wang, H. Wang, P. G. Luo, H. Yang, M. E. Kose, B. Chen, L. M. Veca and S. Y. Xie, *J. Am. Chem. Soc.*, 2006, **128**, 7756–7757.
51 S. J. Zhen, F. L. Guo, L. Q. Chen, Y. F. Li, Q. Zhang and C. Z. Huang, *Chem. Commun.*, 2011, **47**, 2562–2564.

52 D. Kong, F. Yan, Z. Han, J. Xu, X. Guo and L. Chen, *RSC Adv.*, 2016, **6**, 67481–67487.
53 C. L. Li, C. C. Huang, A. P. Periasamy, P. Roy, W. C. Wu, C. L. Hsu and H. T. Chang, *RSC Adv.*, 2015, **5**, 2285–2291.
54 A. H. Gore, D. B. Gunjal, M. R. Kokate, V. Sudarsan, P. V. Anbhule, S. R. Patil and G. B. Kolekar, *ACS Appl. Mater. Interfaces*, 2012, **4**, 5217–5226.
55 J. X. Liu and S. N. Ding, *Anal. Methods*, 2016, **8**, 2170–2175.
56 J. M. Bai, L. Zhang, R. P. Liang and J. D. Qiu, *Chem. – Eur. J.*, 2013, **19**, 3822–3826.
57 L. Zhou, Y. Lin, Z. Huang, J. Ren and X. Qu, *Chem. Commun.*, 2012, **48**, 1147–1149.
58 L. Lin, X. Song, Y. Chen, M. Rong, T. Zhao, Y. Jiang, Y. Wang and X. Chen, *Nanoscale*, 2015, **7**, 15427–15433.
59 Q. Yue, Y. Hou, S. Yue, K. Du, T. Shen, L. Wang, S. Xu, H. Li and J. Liu, *J. Fluoresc.*, 2015, **25**, 585–594.
60 L. L. Tong, Z. Z. Chen, Z. Y. Jiang, M. M. Sun, L. Li, J. Liu and B. Tang, *Biosens. Bioelectron.*, 2015, **72**, 51–55.
61 Z. Hai, Y. Bao, Q. Miao, X. Yi and G. Liang, *Anal. Chem.*, 2015, **87**, 2678–2684.